Applied Energy 88 (2011) 41–51

Contents lists available at ScienceDirect

Applied Energy

journal homepage: www.elsevier.com/locate/apenergy

Comparison of two different flow types on CO removal along a two-stage hydrogen permselective membrane reactor for methanol synthesis

M.R. Rahimpour *, S. Mazinani, B. Vaferi, M.S. Baktash

Chemical Engineering Department, Chemical and Petroleum Engineering School, Shiraz University, Shiraz 71345, Iran

ARTICLE INFO

Article history:
Received 1 February 2010
Received in revised form 22 April 2010
Accepted 25 April 2010
Available online 26 May 2010

Keywords:
CO removal
Hydrogen-permselective membrane
Two-stage membrane reactor
Dynamic model
Catalyst deactivation
Co-current
Counter-current

ABSTRACT

Carbon monoxide (CO) is a gaseous pollutant with adverse effects on human health and the environment. Industrial chemical processes contribute significantly to CO accumulation in the atmosphere. One of the most important processes for controlling carbon monoxide emissions is the conversion of CO to methanol by catalytic hydrogenation. In this study, the effects of two different flow types on the rate of CO removal along a two-stage hydrogen permselective membrane reactor have been investigated. In the first configuration, fresh synthesis gas flows in the tube side of the membrane reactor co-currently with reacting material in the shell side, so that more hydrogen is provided in the first sections of the reactor. In the second configuration, fresh synthesis gas flows in the tube side of the membrane reactor counter-currently with reacting material in the shell side, so that more hydrogen is provided in the last sections of the reactor. For this membrane system, a one-dimensional dynamic plug flow model in the presence of catalyst deactivation was developed. Comparison between co-current and counter-current configurations shows that the reactor operates with higher conversion of CO and hydrogen permeation rate in the counter-current mode whereas; longer catalyst life is achieved in the co-current configuration. Enhancement of CO removal in the counter-current mode versus the co-current configuration results in an ultimate reduction in CO emissions into the atmosphere.

1. Introduction

Carbon monoxide (CO) is a poisonous, colorless, and lethal gas which is a byproduct of incomplete combustion of hydrocarbon-based fuels. This gas has a potential health hazard because when breathed it displaces oxygen in the blood and deprives the heart, brain, and other vital organs of oxygen. Once inside the lungs, CO molecules pass easily into the bloodstream and compete with oxygen for hemoglobin in red blood cells. About 95% of the absorbed CO readily binds with hemoglobin to form carboxyhemoglobin (a compound that inhibits the blood's capacity to carry oxygen to organs and tissues) because the affinity of hemoglobin for CO is over 200 times stronger than it is for oxygen. Thus, the percentage of total hemoglobin in blood that is in the form of carboxyhemoglobin is a biomarker of CO exposure [1,2]. In addition, CO is one of the main reactive trace-gases in the earth's atmosphere. Reduction in CO concentration can significantly counteract the growth of CH_4, so contributes indirectly to global warming and ozone depletion [3–5]. To minimize these effects, carbon monoxide emissions from industrial sources have to be decreased. One possible approach is recycling and fixing CO in a chemical process to form useful products such as methanol that is regarded as an effective method for the reduction of carbon monoxide in the atmosphere. In recent years, a growing interest has been observed in the application of methanol as a green fuel, which can be used directly for powering Otto engines or fuel cells achieving high thermodynamic efficiencies. It can be safely transported by road, rail, barge, ocean tanker or in pipelines. Methanol also contributes significantly to sustainable energy conversion systems as saves a reasonable amount of fossil resources and has almost no impact on the greenhouse effect. The reforming of natural gas is an industrially established process for the production of methanol [6–9]. It is basically synthesized in three steps: synthesis gas generation, methanol synthesis and methanol distillation. Synthesis gas generation accounts for more than 50% of the capital cost of a methanol plant. Synthesis gas consists of CO, CO_2, and H_2 and several inert components like CH_4 and N_2. The main step of methanol process is methanol synthesis. Even though many improvements from its first commercial implementation and a series of new technologies are arising to get it [10], methanol is still largely produced by the natural gas and specifically by means of syngas (CO and H_2 mixture) obtained via steam reforming operations.

At the entrance of methanol reactors, the reactions are rate-base, so increasing temperature enhances rate of reaction and CO conversion. At the exit of the reactor, however, the reactions are

* Corresponding author. Tel.: +98 76 2303071; fax: +98 76 6287294.
E-mail address: rahimpor@shirazu.ac.ir (M.R. Rahimpour).

0306-2619/$ - see front matter © 2010 Elsevier Ltd. All rights reserved.
doi:10.1016/j.apenergy.2010.04.022

Nomenclature

A_c	cross section area of each tube (m^2)
A_i	inner area of each tube (m^2)
A_o	outside area of each tube (m^2)
A^{sh}	cross section area of shell (m^2)
a	activity of catalyst (–)
a_v	specific surface area of catalyst pellet ($m^2\ m^{-3}$)
c_{pg}	specific heat of the gas at constant pressure ($J\ mol^{-1}\ k^{-1}$)
c_{ph}	specific heat of the hydrogen at constant pressure ($J\ mol^{-1}\ k^{-1}$)
c_{ps}	specific heat of the catalyst at constant pressure ($J\ mol^{-1}\ k^{-1}$)
c_t	total concentration ($mol\ m^{-3}$)
D	reactor diameter (m)
D_i	tube inside diameter (m)
D_{ij}	binary diffusion coefficient of component i in j ($m^2\ s^{-1}$)
D_m^i	diffusion coefficient of component i in the mixture ($m^2\ s^{-1}$)
D_o	tube outside diameter (m)
d_p	particle diameter (m)
E_d	activation energy used in the deactivation model ($J\ mol^{-1}$)
F^{sh}	total molar flow in shell side ($mol\ s^{-1}$)
F^{tu}	total molar flow per tube ($mol\ s^{-1}$)
f_i	partial fugacity of component i (bar)
h_f	gas-catalyst heat transfer coefficient ($W\ m^{-2}\ K^{-1}$)
h_i	heat transfer coefficient between fluid phase and reactor wall ($W\ m^{-2}\ K^{-1}$)
h_o	heat transfer coefficient between coolant stream and reactor wall ($W\ m^{-2}\ K^{-1}$)
K	conductivity of fluid phase ($W\ m^{-1}\ K^{-1}$)
K_d	deactivation model parameter constant (s^{-1})
K_i	adsorption equilibrium constant for component i (bar^{-1})
K_{pi}	equilibrium constant based on partial pressure for component i (–)
K_w	thermal conductivity of reactor wall ($W\ m^{-1}\ K^{-1}$)
k_1	reaction rate constant for the 1st rate equation ($mol\ kg^{-1}\ s^{-1}\ bar^{-1/2}$)
k_2	reaction rate constant for the 2nd rate equation ($mol\ kg^{-1}\ s^{-1}\ bar^{-1/2}$)
k_3	reaction rate constant for the 3rd rate equation ($mol\ kg^{-1}\ s^{-1}\ bar^{-1/2}$)
k_{gi}	mass transfer coefficient for component i ($m\ s^{-1}$)
L	length of reactor (m)
M_i	molecular weight of component i ($g\ mol^{-1}$)
N	number of components (–)
N_i	molar flux ($mol\ s^{-1}\ m^{-2}$)
P	total pressure (bar)
P_a	atmospheric pressure (bar)
P_H^{tu}	tube side pressure (bar)
P_H^{sh}	shell side pressure (bar)
Ps^-	permeability of hydrogen through Pd–Ag layer ($mol\ m^{-1}\ s^{-1}\ Pa^{-1/2}$)
P_0	pre-exponential factor of hydrogen permeability ($mol\ m^{-1}\ s^{-1}\ Pa^{-1}$)
R	universal gas constant ($J\ mol^{-1}\ K^{-1}$)
R_e	Reynolds number (–)
R_i	inner radius of Pd–Ag layer (m)
R_o	outer radius of Pd–Ag layer (m)
r_i	reaction rate of component i ($mol\ kg^{-1}\ s^{-1}$)
r_1	rate of reaction for hydrogenation of CO ($mol\ kg^{-1}\ s^{-1}$)
r_2	rate of reaction for hydrogenation of CO_2 ($mol\ kg^{-1}\ s^{-1}$)
r_3	reversed water–gas shift reaction ($mol\ kg^{-1}\ s^{-1}$)
Sc_i	Schmidt number of component i (–)
T	bulk gas phase temperature (K)
T_R	reference temperature used in the deactivation model (K)
T_s	temperature of solid phase (K)
T_{sat}	saturated temperature of boiling water at operating pressure (K)
T^{sh}	temperature of coolant stream, in first reactor (K)
T^{tu}	temperature of coolant stream, in second reactor (K)
t	Time (s)
U^{sh}	overall heat transfer coefficient between coolant and process streams ($W\ m^{-2}\ K^{-1}$)
U	superficial velocity of fluid phase ($m\ s^{-1}$)
u_g	linear velocity of fluid phase ($m\ s^{-1}$)
y_i^{sh}	mole fraction of component i in the fluid phase in shell ($mol\ mol^{-1}$)
y_{is}^{sh}	mole fraction of component i in the solid phase in shell
y_i^{tu}	mole fraction of component i in the fluid phase in tube side ($mol\ mol^{-1}$)
y_{is}^{tu}	mole fraction of component i in the solid phase in tube side ($mol\ mol^{-1}$)
z	axial reactor coordinate (m)

Greek letters

α_H	hydrogen permeation rate constant ($mol\ m^{-1}\ s^{-1}\ Pa^{-0.5}$)
$\Delta H_{f,i}$	enthalpy of formation of component i ($J\ mol^{-1}$)
ΔH_{298}	enthalpy of reaction at 298 K ($J\ mol^{-1}$)
ε_B	void fraction of catalytic bed (–)
ε_s	void fraction of catalyst (–)
μ	viscosity of fluid phase ($kg\ m^{-1}\ s^{-1}$)
ν	stoichiometric coefficient (–)
v_{ci}	critical volume of component i ($cm^3\ mol^{-1}$)
ρ	density of fluid phase ($kg\ m^{-3}$)
ρ_B	density of catalytic bed ($kg\ m^{-3}$)
ρ_s	density of catalyst ($kg\ m^{-3}$)
η	catalyst effectiveness factor (–)
τ	tortuosity of catalyst (–)
Ω	auxiliary variable (–)
Δ	thickness of membrane (m)

Superscripts and subscripts

i	component i
f	feed conditions
p	permeation side
in	inlet conditions
out	outlet conditions
k	reaction number index (1, 2 or 3)
s	at catalyst surface
sh	shell side
ss	initial conditions (i.e., steady-state condition)
tu	tube side

equilibrium-based and an increase in temperature decreases the equilibrium conversion of CO. Therefore, achieving the highest temperature at the entrance with a gradual decrease toward the exit of the reactor in order to reach the highest removal rate of CO is a major issue in methanol synthesis.

Recently, a two-stage (instead of a single-type) methanol synthesis reactor has been introduced by Lurgi for CO conversion to methanol [11]. This system represents an advanced technology for converting synthesis gas to methanol at low cost and in large quantities. The system basically consists of two reactors. The first

is a high temperature water-cooled reactor that is combined in series with a low temperature gas-cooled reactor where partial conversion of CO to methanol is achieved. Reacting gas in the second reactor has low H_2 content resulting in a decreased performance in comparison with the first reactor. One way to enhance the performance of the gas-cooled reactor is to add hydrogen to the reacting gas selectively by using a membrane, shifting the chemical equilibrium towards the product side [12].

A membrane two-stage methanol synthesis reactor has been developed by Rahimpour and Lotfinejad [13]. This modified reactor combines the chemical and membrane conversion in one system and has these advantages: (1) Enhancement of CO conversion, overcoming the potential limitations imposed by thermodynamic equilibrium [12]; (2) Higher CO conversion relative to CO_2 conversion so that little water is produced during methanol synthesis; (3) Improvement of kinetics-limited reactions in the first reactor as a result of higher feed temperature; (4) Enhancement of equilibrium-limited reactions due to a lower temperature in the second reactor; (5) Control of the stoichiometric number of reacting gases along the gas-cooled reactor by hydrogen diffusion through the membrane. In chemical processes, membrane conversion technologies are mainly used in reaction systems containing hydrogen and oxygen where inorganic membranes are dominantly implemented [14]. It has been observed that diffusion of hydrogen through palladium membranes can enhance the selectivity of hydrogenation [15]. The use of Pd membranes is hindered because palladium shows a transition from the α-phase (hydrogen poor) to the β-phase (hydrogen rich) at temperatures below 300 °C and pressures below 2 MPa, depending on the hydrogen concentration in the metal. Since the lattice constant of the α-phase is 3% smaller than that of the β-phase, this transition leads to lattice strain, and consequently after a few cycles, to a deformity of the metal lattice [16]. In many hydrogen-related reaction systems, Pd-alloy membranes on a stainless steel support have been used as the hydrogen-permeable membrane [17]. A maximum value of hydrogen permeability is reached for an alloy with a silver content of 23 wt.% [18]. Despite numerous membranes developed and investigated, Pd and its alloy membranes are still the most widely employed membranes for transporting hydrogen because of their high permeability and selectivity, good surface properties and ability to catalyze the surface dissociation and reassociation of H_2 [19,20]. These membranes combine hydrogen transition with distinguishing properties such as resistance to high temperatures, solvents, and corrosion. The main reason for the development of Pd-based membranes is low costs as well as perm-selectivity combined with good mechanical, thermal and long-term stability [21]. Thick-walled palladium alloy membranes have shown good thermal stability against high temperature and the reactant atmospheres, in some studies with thin palladium or palladium alloy films deposited by electroless plating stability problems have been encountered at temperatures above 400–500 °C. These properties make palladium-based membranes, such as Pd–Ag membranes, interesting alternatives for use in the petrochemical industry.

Membrane two-stage methanol synthesis reactors are similar to their conventional counterparts with the exception that in this system, the walls of tubes in the gas-cooled reactor are coated with a Pd–Ag membrane. Generally, feed synthesis gas can be introduced into the gas-cooled reactor with two different flow configurations in relation to the reacting gas flow – co-current (in parallel flow) and counter-current (in counter-flow) [22–24].

In previous works, the authors have studied co-current and counter-current modes of operation for an industrial and fluidized-bed membrane two-stage methanol synthesis reactor [25,26]. These studies revealed that implementing a counter-current flow configuration yields higher methanol production than when a co-current configuration is used.

The objective of the present study is to compare the performance of membrane two-stage methanol synthesis reactors in co-current and counter-current configurations in terms of CO removal rates, catalyst activity and hydrogen permeation rates. This comparison shows that the counter-current mode yields a higher conversion of CO with a higher CO removal rate and higher hydrogen permeation rate compared with the co-current mode. However, in the co-current mode, the catalyst activity is maintained at higher levels resulting in longer catalyst life.

2. Reactor configurations

2.1. Conventional two-stage methanol synthesis reactor

The catalyst is packed in vertical tubes of the gas-cooled reactor and the shell side of water-the cooled reactor. Reactions of methanol synthesis are performed over commercial $CuO/ZnO/Al_2O_3$ catalysts. Cold feed synthesis gas is fed to tubes of the second reactor and is flowing in counter-current mode with methanol-containing reacting gas in the shell of the same reactor. Outlet synthesis gas then enters the tubes of the first reactor and the chemical reaction is initiated by the catalyst. The remaining heat of reaction is transferred to the cooling water inside the shell. In this stage, CO is partly converted to methanol. Then the reacting gas mixture is left directing to the catalyst shell side of the second reactor and its temperature is continuously reduced through the catalyst bed. Finally, the product is removed from the side stream of the second reactor.

In general, temperature of the first reactor is higher than that of the second reactor so the main catalyst deactivation occurs in this reactor and the lower operating temperature in the gas-cooled reactor results in a practically unlimited catalyst service life. In addition, reaction control extends catalyst life of the water-cooled reactor.

The input data and industrial design of the catalyst pellet for the industrial two-stage methanol synthesis reactor have been listed in Tables 1 and 2.

2.2. Membrane two-stage methanol synthesis reactor in co-current and counter-current modes

Methanol synthesis in membrane two-stage reactors is similar to their conventional two-stage counterparts, with the exception that in the membrane system, the walls of tubes in the gas-cooled reactor are coated with a hydrogen perm-selective membrane. The pressure difference between the shell (71.2 bar) and tubes (76.98 bar) in the membrane two-stage reactor permits hydrogen diffusion through the Pd–Ag membrane layer. On the other hand, in this system, mass and heat transfer occur simultaneously be-

Table 1
Specifications of catalyst and reactor of conventional two-stage methanol synthesis.

Water-cooled reactor		Gas-cooled reactor	
Parameter	Value	Value	Unit
D	4.5	5.5	[m]
D_i	40.3	21.2	[mm]
D_o	4.5	25.4	[mm]
d_p	0.00574	0.00574	[m]
ρ_s	1770	1770	[kg m^{-3}]
c_{ps}	5.0	5.0	[kJ kg^{-1} K^{1}]
λ_c	0.004	0.004	[W m^{-1} K^{-1}]
a_v	625.7	625.7	[m^2 m^{-3}]
ε_s	0.39	0.39	[–]
ε_B	0.39	0.39	[–]
Tube length	8	10	[m]
Number of tubes	5955	3026	[–]
Shell side pressure	–	71.2	[bar]
Tube side pressure	75	76.98	[bar]

Table 2
Input data of the industrial two-stage methanol synthesis reactor.

Feed conditions	Value
Feed composition (mol%):	
CO	8.68
CO_2	8.49
H_2	64.61
CH_4	9.47
N_2	8.2
H_2O	0.1
CH_3OH	0.37
Argon	0.24
Inlet temperature [K]	401
Total molar flow rate per tube (mol/s)	7.1
Pressure [bar]	76

tween the shell and the tubes, while in the conventional-type only a heat transfer occurs between them.

The difference between methanol synthesis in counter-current and co-current modes is in the direction of synthesis gas flowing through the tubes of the second reactor. In counter-current configuration, feed synthesis gas is fed to the tubes in opposite direction to the reacting gas from the top of the reactor, whereas in co-current configuration, synthesis gas flows through the tubes in the same direction as the reacting gas mixture stream in the shell side. Fig. 1 is a schematic diagram of a membrane two-stage methanol synthesis reactor in counter-current and co-current modes for CO conversion to methanol.

In this simulation study, the Pd–Ag layer thickness is 0.8 mm and all specifications for the membrane two-stage system in the first and second reactors are the same as conventional reactors as summarized in Tables 1 and 2.

3. Mathematical model

The mathematical model for the simulation of the membrane two-stage methanol synthesis reactor was developed based on the following assumptions: (1) All streams are considered as one-dimensional plug flow; (2) Axial dispersion of heat is negligible compared with convection; (3) Gases are ideal; (4) Radial diffusion in the catalyst pellet is neglected; (5) There are no radial concentration and temperature gradients; (6) The axial diffusion of hydrogen through the membrane is neglected compared to the radial diffusion; Fig. 2 is the schematic diagram of an elemental volume of a membrane reactor in co-current and counter-current modes.

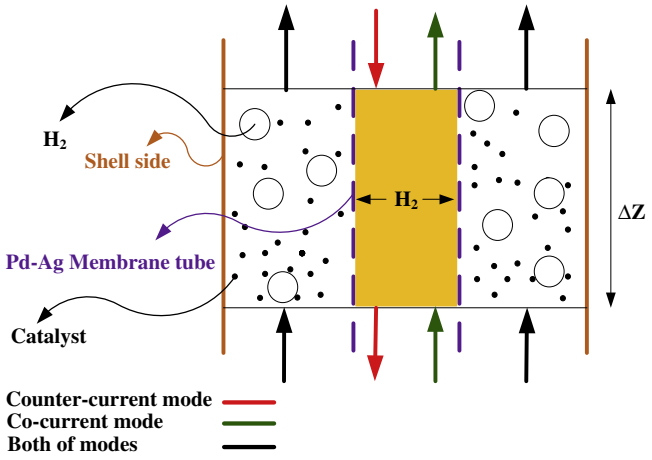

Fig. 2. Schematic diagram of an element volume of a membrane reactor in co-current and counter-current modes.

3.1. Water-cooled reactor (first stage)

In the tube side, mass and energy balance for solid phase are expressed by:

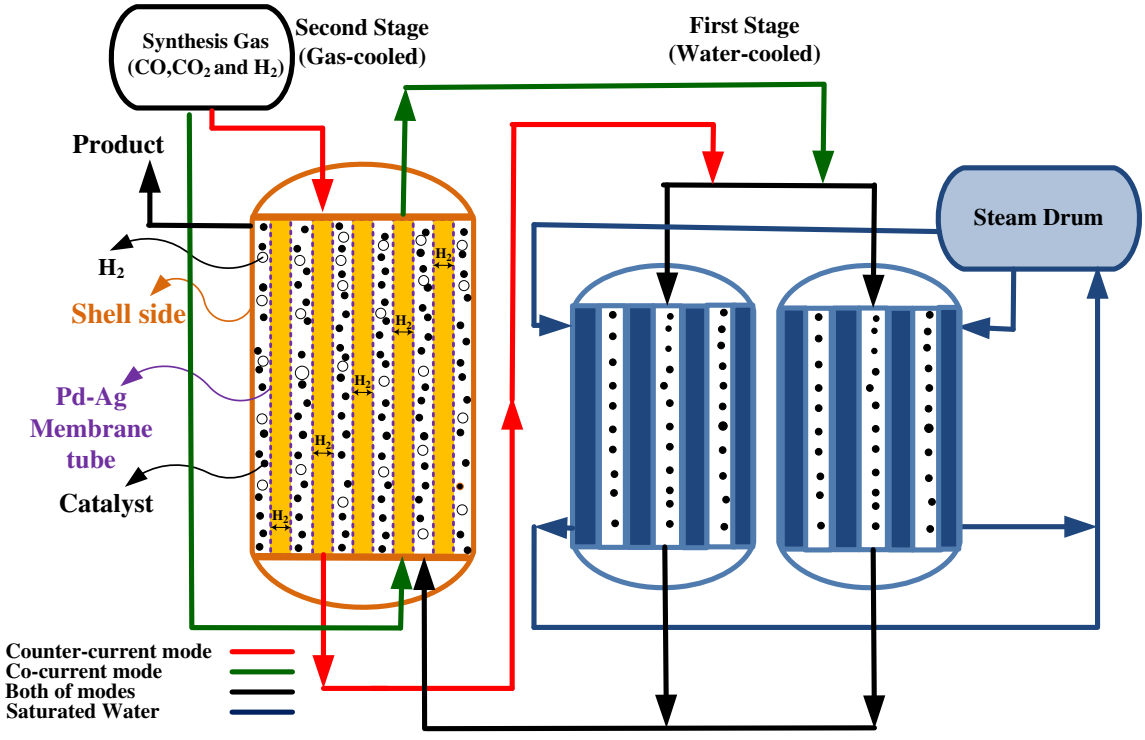

Fig. 1. Schematic diagram of a membrane two-stage methanol synthesis reactor in counter-current and co-current configurations.

$$\varepsilon_s c_t \frac{\partial y_{is}^{tu}}{\partial t} = k_{g_i}(y_i^{tu} - y_{is}^{tu}) + \eta r_i \rho_B a \quad i = 1,2,\ldots,N-1 \tag{1}$$

$$\rho_B c_{ps} \frac{\partial T_s^{tu}}{\partial t} = a_v h_f (T^{tu} - T_s^{tu}) + \rho_B a \sum_{i=1}^{N} \eta r_i (-\Delta H_{f,i}) \tag{2}$$

where y_{is}^{tu} and T_s^{tu} are the mole fraction and temperature of the solid-phase in the tube side, respectively, and i represents CH_3OH, CO, CO_2, H_2, H_2O. Argon, Nitrogen and Methane are inert components. The following two conservation equations are written for the fluid phase:

$$\varepsilon_B c_t \frac{\partial y}{\partial t} = -\frac{F^{tu}}{A_c}\frac{\partial y_i^{tu}}{\partial z} + a_v c_t k_{g_i}(y_{is}^{tu} - y_i^{tu}) \quad i = 1,2,\ldots,N-1 \tag{3}$$

$$\varepsilon_B c_t c_{pg} \frac{\partial T^{tu}}{\partial t} = -\frac{F^{tu}}{A_c}\frac{\partial T^{tu}}{\partial z} + a_v h_f (T_s^{tu} - T^{tu}) + \frac{\pi D_i}{A_c} U^{sh}(T^{sh} - T^{tu}) \tag{4}$$

where y_i^{tu} and T^{tu} are the fluid-phase mole fraction and temperature in the tube side; Also F^{tu} and A_c are total molar flow rate and cross-section in each tube, respectively. The boundary conditions are unknown and further details are discussed in the section concerning the numerical solution.

$$z = 0; \quad F^{tu} = F_{in}, \quad y_i^{tu} = y_{i_{in}}, \quad T^{tu} = T_{in} \tag{5}$$

The initial conditions are:

$$t = 0; \quad y_i^{tu} = y_i^{ss}, \quad y_{is}^{tu} = y_{is}^{ss}, \quad T^{tu} = T^{ss}, \quad T_s^{tu} = T_s^{ss}, \quad a = 1 \tag{6}$$

3.2. Gas-cooled reactor (second stage)

3.2.1. Shell side

Overall mass balance:

$$\varepsilon_B \frac{\partial c_t}{\partial t} = -\frac{1}{A^{sh}}\frac{\partial F^{sh}}{\partial z} + \frac{\alpha_H}{A^{sh}}\left(\sqrt{P_H^{tu}} - \sqrt{P_H^{sh}}\right) \tag{7}$$

where c_t, F^{sh} are total concentration and flow rate of the reacting gas mixture in the shell side. A^{sh} is the cross-sectional area of shell and α_H is rating constant of hydrogen permeation. P_H^{tu} and P_H^{sh} are partial pressures of hydrogen in tube and shell sides, respectively. Mass and energy balance in the gas-cooled reactor for the solid phase are the same as in the water-cooled reactor. The following equations are written for the fluid phase:

$$\varepsilon_B c_t \frac{\partial y_i^{sh}}{\partial t} = -\frac{1}{A^{sh}}\frac{\partial F_i^{sh}}{\partial z} + a_v c_t k_{gi}(y_{is}^{sh} - y_i^{sh}) + \frac{\alpha_H}{A^{sh}}\left(\sqrt{P_H^{tu}} - \sqrt{P_H^{sh}}\right) \quad i = 1,2,\ldots,N-1 \tag{8}$$

$$\varepsilon_B c_t c_{pg} \frac{\partial T^{sh}}{\partial t} = -\frac{1}{A^{sh}} C_{pg} \frac{\partial (F^{sh} T^{sh})}{\partial z} + a_v h_f (T_s^{sh} - T^{sh}) + \frac{\alpha_H}{A^{sh}}\left(\sqrt{P_H^{tu}} - \sqrt{P_H^{sh}}\right) c_{ph}(T^{tu} - T^{sh}) + \frac{\pi D_i}{A^{sh}} U^{tu}(T^{tu} - T^{sh}) \tag{9}$$

Mass and energy balance for the solid phase are written as:

$$\varepsilon_s c_t \frac{\partial y_{is}^{sh}}{\partial t} = k_{g_i}(y_i^{sh} - y_{is}^{sh}) + \eta r_i \rho_B a \quad i = 1,2,\ldots,N-1 \tag{10}$$

$$\rho_B c_{ps} \frac{\partial T_s^{sh}}{\partial t} = a_v h_f (T^{sh} - T_s) + \rho_B a \sum_{i=1}^{N} \eta r_i (-\Delta H_{f,i}) \tag{11}$$

where y_i^{sh} and T_s^{sh} are the mole fraction and temperature of the solid phase in the shell side, respectively.

3.2.2. Tube side

Overall mass balance:

$$\frac{\partial c_t}{\partial t} = \pm\frac{1}{A_c}\frac{\partial F^{tu}}{\partial z} - \frac{\alpha_H}{A_c}\left(\sqrt{P_H^{tu}} - \sqrt{P_H^{sh}}\right) \tag{12}$$

where c_t and F^{tu} are total concentration and flow rate in the tube side. Mass and energy balance equations for the fluid phase are given as:

$$c_t \frac{\partial y_i^{tu}}{\partial t} = \pm\frac{1}{A_c}\frac{\partial F_i^{sh}}{\partial z} - \frac{\alpha_H}{A_c}\left(\sqrt{P_H^{tu}} - \sqrt{P_H^{sh}}\right) \quad i = 1,2,\ldots,N-1 \tag{13}$$

$$c_t c_{p_g} \frac{\partial T^{tu}}{\partial t} = \pm\frac{1}{A_c} C_{pg} \frac{\partial (F^{tu} T^{tu})}{\partial z} + \frac{\pi D_i}{A_c} U^{tu}(T^{sh} - T^{tu}) + \frac{\alpha_H}{A_c}\left(\sqrt{P_H^{tu}} - \sqrt{P_H^{sh}}\right) C_{ph}(T^{sh} - T^{tu}) \tag{14}$$

The boundary conditions are as follows:

$$z = L; \quad y_i^{tu} = y_{if}, \quad T^{tu} = T_f \tag{15}$$

when $\alpha_H = 0$, the membrane is not permeable to hydrogen and the model is used for conventional two-stage systems.

3.3. Equilibrium model

Equilibrium conversions can be calculated by solving two reaction equilibrium expressions simultaneously. Equilibrium constants for reactions (A1) and (A2), which are presented in Appendix A, are as follows:

$$K_{p1} = \frac{F_{CH_3OH}(F)^2}{F_{CO}(F_{H_2})^2 (P)^2} \tag{16}$$

$$K_{P2} = \frac{F_{CO} F_{H_2O}}{F_{CO_2} F_{H_2}} \tag{17}$$

Reaction (A3) is not necessary for thermodynamic analysis because it is a linear combination of the first two reactions – (A1) and (A2) [27]. The equilibrium constants of reactions (A1) and (A3), K_{p1} and K_{p3}, have been identified as functions of temperature and pressure by Klier et al. [28]:

$$K_{p1} = \frac{3.27 \times 10^{-13} \exp(11,678/T)}{1 - (1.95 \times 10^{-4} \exp(1703/T))P} \tag{18}$$

$$K_{p3} = \frac{3.823 \times 10^{-13} \exp(11,678/T)}{1 - (1.95 \times 10^{-4} \exp(1703/T)P)(1 - 4.24 \times 10^{-4} \exp(1107/T)P)} \tag{19}$$

K_{p2} is obtained from K_{p1} and K_{p3} by the equilibrium relationship:

$$K_{P2} = \frac{K_{P3}}{K_{P1}} \tag{20}$$

These equations can be applied to estimate equilibrium conversion by defining X_e and Y_e as the moles of CH_3OH and H_2O formed, respectively. These are used for membrane methanol reactors and when there is no membrane, the term $F_{H_2,in}^p - F_{H_2,out}^p$, which represents additional hydrogen in reacting gas, is zero. Material balances around the methanol reactor are:

$$F_{CH_3OH} = F_{CH_3OH,in} + X_e \tag{21}$$

$$F_{H_2O} = F_{H_2O,in} + Y_e \tag{22}$$

$$F_{CO_2} = F_{CO_2,in} - Y_e \tag{23}$$

$$F_{CO} = F_{CO,in} - X_e + Y_e \tag{24}$$

$$F_{H_2} = F_{H_2,in} - 2X_e - Y_e + F_{H_2,in}^p - F_{H_2,out}^p \tag{25}$$

$$F_{N_2} = F_{N_2,in} \tag{26}$$

Summation of Eqs. (19)–(24) results in the total flow rate of reaction side gas:

$$F_T = F_{in} - 2X_e + F^p_{H_2,in} - F^p_{H_2,out} \quad (27)$$

Substitution of Eqs. (16)–(25) into Eqs. (14) and (15) yields two equations with two unknown extents of reaction, X_e and Y_e. These equations can be solved numerically, but it has been discovered advantageous to work with the logarithms of both. The resulting equations used in the calculations are:

$$F_1(X,Y) = \ln(K_{p1}) - \ln\left(\frac{(F_{CH_3OH})(F)^2}{(F_{CO})(F_{H_2})^2(P)^2}\right) \quad (28)$$

$$F_2(X,Y) = \ln(K_{p2}) - \ln\left(\frac{F_{CO}F_{H_2O}}{F_{CO_2}F_{H_2}}\right) \quad (29)$$

Generally, convergent multi-dimensional Newton's method in Fortran PowerStation 4.0 numerical recipes was used to solve the model equilibrium Eqs. (28) and (29).

3.4. Deactivation model

The deactivation model of the $CuO/ZnO/Al_2O_3$ catalyst has been studied by several researchers; however, the model suggested by Hanken was found to be suitable for industrial applications [29]:

$$\exp\left(\frac{-E_d}{R}\left(\frac{1}{T} - \frac{1}{T_R}\right)\right)a^5\frac{da}{dt} = -K_d \quad (30)$$

where E_d, T_R and K_d are activation energy, reference temperature and catalyst deactivation constant, respectively. The numerical value of E_d is 91,270 J/mol, T_R is 513 K and K_d is 0.00439 h^{-1} [29]. The above model has been fitted with industrial operating conditions and is the only case for simulation and modeling of industrial plants.

3.5. Hydrogen permeation in the Pd/Ag membrane

The flux of hydrogen permeating through the palladium membrane (j) depends on the difference in the partial pressure of hydrogen on the two sides of the membrane. Here, hydrogen permeation is determined assuming Sieverts' law:

$$j_H = \alpha_H\left(\sqrt{P^{tu}_H} - \sqrt{P^{sh}_H}\right) \quad (31)$$

Data for the diffusion of hydrogen through Pd–Ag membrane were determined experimentally. In Eqs. (7)–(12), α_H is hydrogen permeation rate constant and is defined as [30]:

$$\alpha_H = \frac{2\pi L\bar{P}}{\ln}\left(\frac{R_o}{R_i}\right) \quad (32)$$

where R_o (0.027), R_i (0.027008) represent outer and inner radii of the Pd–Ag layer. Here, the hydrogen permeability through the Pd–Ag layer is determined assuming Arrhenius law, which is a function of temperature as follows [31,32]:

$$\bar{P} = P_0\exp\left(\frac{-E_p}{RT}\right) \quad (33)$$

where the pre-exponential factor P_0 above 200 °C is reported as 6.33×10^{-8} (mol/m^2 s Pa$^{1/2}$) and activation energy E_p is 15.7 kJ/kmol [31,32].

4. Numerical solution

The fundamental structure of the model includes partial derivative equations of mass and energy conservation in solid and fluid phases, which have to be coupled with the ordinary differential equation of the deactivation model, and also non-linear algebraic equations of the kinetic model and auxiliary correlations. The equations are solved using a two-stage approach consisting of a steady-state simulation stage followed by a dynamic solution stage. In order to solve the set of reactor model equations, a steady-state simulation has been used prior to a dynamic simulation that exports initial values to the dynamic simulator.

4.1. Steady-state simulation

Steady-state model solution of the two-stage methanol reactor is performed by equaling all the time-variation of the states to zero and also considering a fresh catalytic bulk with the activity of unity. In this way, the initial conditions for temperature and concentration are determined for the dynamic simulation.

After rewriting the model equations, a set of differential algebraic equations (*DAEs*) is obtained for both co-current and counter-current modes. This set of equations is changed to non-linear algebraic equations (*NAEs*) using backward finite difference approximation. The *NAEs* are boundary value problem which has been solved using the shooting method in counter-current mode and trial and error method in co-current mode.

4.1.1. Solution procedure for co-current mode

In co-current mode, the calculation was started with initial guesses for T_{in} and y_{in}, which are unknown (initial conditions). The initial conditions were calculated using the Gauss–Newton method replaced by its previous value in subsequent calculations. Substitution was continued until the convergence criterion was met.

4.1.2. Solution procedure for counter-current mode

In counter-current mode, the inlet feed synthesis gas temperature (T_{in}) and hydrogen mole fraction (y_{in}) to the water-cooled reactor are unknown (initial conditions), whereas the temperature (T_f) and hydrogen mole fraction (y_f) of the feed synthesis gas stream to the gas-cooled are known (final condition). The shooting method converts the boundary-value problem to an initial-value problem. Solution is possible by guessing values for T_{in} and y_{in} for the heated feed synthesis gas to the first stage. The first and second stages were divided into 14 and 16 nodes, respectively, and then the Gauss–Newton method was used to solve the nonlinear algebraic equations in each node. In the end, the calculated values of temperature (T_f) and hydrogen mole fraction (y_f) of the fresh feed synthesis gas were compared with the actual values. This procedure was repeated until the specified terminal values were obtained within a small convergence criterion.

4.2. Solution of the dynamic model

The results of steady-state simulations are used as initial conditions for time integration of dynamic state equations in each node through the two-stage methanol synthesis reactor. The set of dynamic equations of the deactivation model and conservation laws consist of simultaneous ordinary and partial differential equations, as well as algebraic equations due to auxiliary correlations, kinetics and thermodynamics of the reaction system. The set of equations

Table 3
Comparison between model results with plant date for fresh catalyst.

Product condition	Plant	Predicted	Error (%)
Composition (mol%):			
CH_3OH	0.104	0.1023	−3.4
CO	0.0251	0.0228	−4.38
CO_2	0.0709	0.0764	−9.16
H_2O	0.0234	0.0211	−9.82
H_2	0.5519	0.5323	−3.55
N_2/Ar	0.0968	0.0905	−6.5
CH_4	0.114	0.103	−9.64
Temperature [K]	495	489.5	−1.2
CO removal rate [tons/day]	4465	4542.2	1.7

have been separated with respect to the axial coordinate. Modified Rosenbrock formula of order 2 has been applied to discrete equations in each node along the reactor to integrate the set of equations with respect to time. The process duration has been considered to be 1400 operating days.

Table 4
Comparison between predicted methanol production rate and plant data.

Time (day)	Plant (ton/day)	Predicted (ton/day)	Error (%)
0	295.0	308.80	2.93
100	296.5	297.03	0.18
200	302.6	289.10	−4.46
300	284.3	283.09	−0.44
400	277.9	278.19	0.10
500	278.2	274.03	−1.50
600	253.0	270.41	6.88
700	274.0	267.19	−2.48
800	268.1	264.30	−1.65
900	275.5	261.67	−5.02
1000	274.6	259.25	−5.58
600	262.9	257.02	−2.24
1200	255.2	255.18	−0.05

5. Results and discussion

5.1. Model validation

The validation of steady-state and dynamic models for co-current and counter-current configurations along the conventional two-stage methanol synthesis reactor with plant data has previously been performed by Rahimpour et al. and good agreement between the daily plant data and the simulation data was observed [25].

5.1.1. Steady-state model validation

The steady-state model was validated by comparing its results at time zero ($t = 0$) with plant data for a conventional two-stage methanol synthesis reactor ($\alpha_H = 0$) under design specifications. Input data is presented in Tables 1 and 2, respectively. The model results and data of the plant are tabulated in Table 3. It was observed that the steady-state model functioned acceptably under industrial conditions and the results of simulations were in good agreement with daily-real plant data.

5.2. Dynamic model validation

Validation of the dynamic model was performed by comparing simulation results with process history data of a single-type meth-

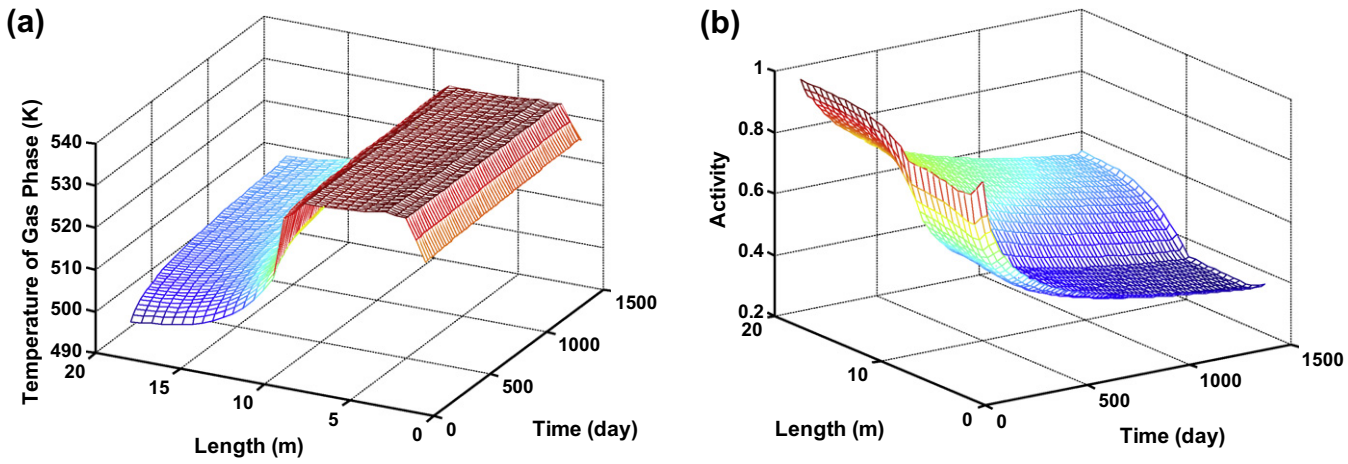

Fig. 3. Profiles of (a) temperature and (b) catalyst activity versus time and length for a membrane two-stage methanol synthesis reactor in co-current mode.

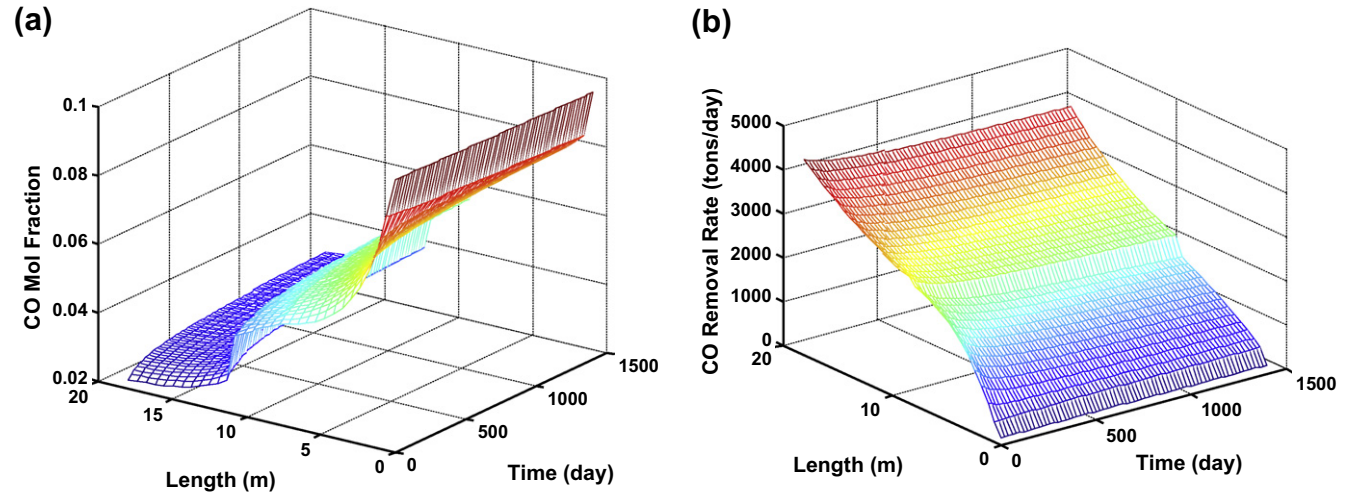

Fig. 4. Profiles of (a) CO removal rate and (b) CO mole fraction versus time and length.

anol synthesis reactor. The predicted results for the production rate and the corresponding observed data of the plant are listed in Table 4. It was demonstrated that the model carried out satisfactorily under industrial conditions and a good agreement was observed between the simulation data and daily plant data.

A parametric analysis was performed to address the vital issues, such as CO mole fraction, CO removal rate, temperature and catalyst activity profiles along the reactor. Fig. 3a and b illustrates the reactor temperature and catalyst activity profiles versus time and length in co-the current mode for a membrane two-stage methanol

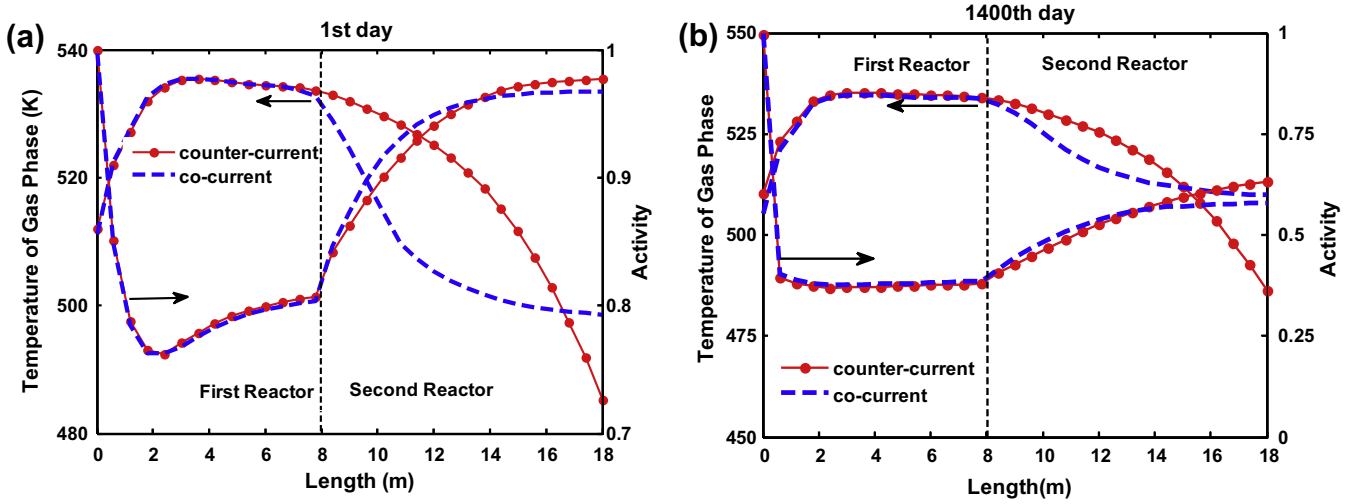

Fig. 5. Profiles of the temperature and activity along co-current and counter-current reactor configurations for (a) 1st and (b) 1400th days.

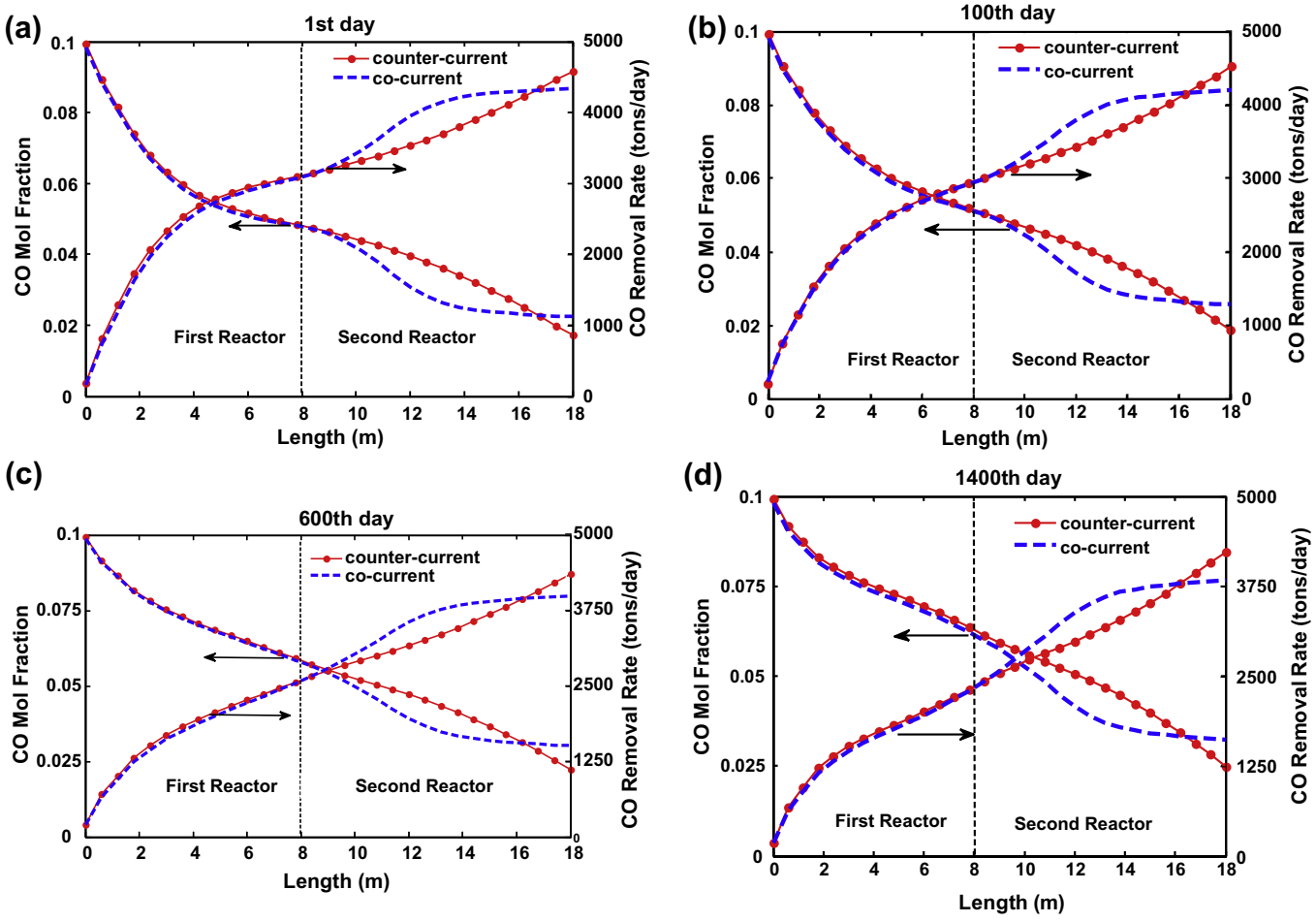

Fig. 6. Profiles of the CO mole fraction and removal rate along co-current and counter-current reactor configurations for (a) 1st, (b) 100th, (c) 600th, and (d) 1400th days.

synthesis reactor. In the first stage, temperature of the reacting gas mixture in first days is higher than in the second stage due to higher conversion and freshness of catalyst. Moreover, temperature of the reacting gas mixture in both stages decrease with time because the heat of reaction is continuously removed by the water and gas coolants. However, the capability of the coolant gas to remove reaction heat is less than coolant water, as shown in Fig. 3a. Minimum activity is observed near the first reactor inlet, which is exposed to higher temperatures at different times. In the gas-cooled reactor, catalyst must have a lower temperature, which improves catalyst activity and the equilibrium constant, as shown in Fig. 3b. Also, this figure shows that during the operating time, the catalyst is deactivated as a result of poisoning and thermal sintering – the loss of catalyst active surface area owing to crystallite growth of either the support material or the active phase.

Fig. 4a and b is a three-dimensional plot of CO mol fraction and CO removal rate along the reactor length and time in co-current configuration for a two-stage membrane methanol synthesis reactor. CO mole fraction decreases along the reactor and increases with time because of catalyst deactivation, as shown in Fig. 4a. On the other hand, CO removal rate increases along the reactor and decreases as time passes (see Fig. 4b).

5.3. Comparison of co-current and counter-current modes

Fig. 5a and b shows the comparison between the temperature and catalyst activity profiles along co-current and counter-current reactor configurations for the 1st and the 1400th days. As can be seen in this figure, the first reactor operates at a lower temperature in the co-current mode compared with the counter-current configuration because feed synthesis gas in this stage is preheated more efficiently in the counter-current mode along the second stage. The gas-cooled reactor operates at a higher temperature in the counter-current mode than in the co-current mode, while an inverse behavior is observed near the reactor outlet. The lower temperature in most segments of the co-current configuration enhances catalyst activity, which results in a more effective use of the catalyst. Therefore, the reactor supplies a favorable catalyst activity in the co-current mode in comparison with the counter-current mode.

The CO mole fraction and removal rate of CO profiles in co-current and counter-current modes for the 1st, 100th, 600th and 1400th days of operation have been compared in Fig. 6a–d.

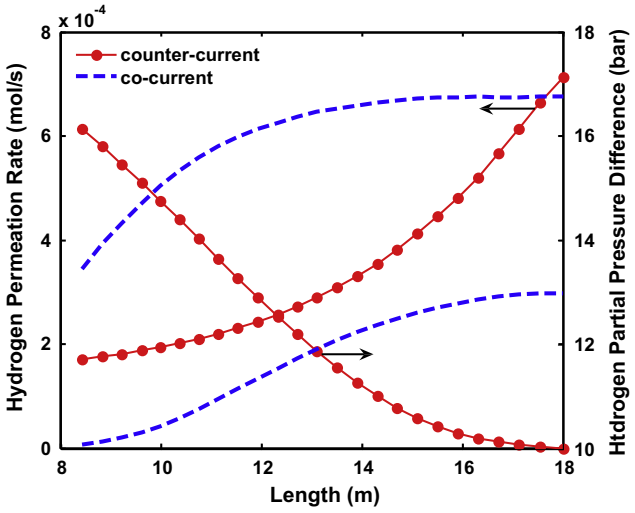

Fig. 7. Profiles of hydrogen permeation rate and partial pressure difference along the reactor in co-current and counter-current modes for fresh catalyst.

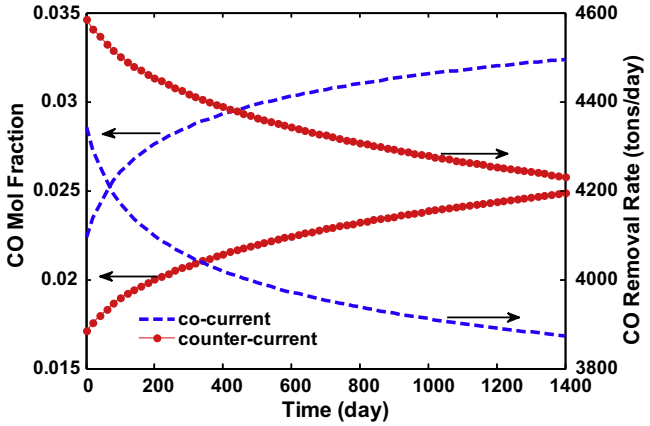

Fig. 8. Comparison of CO mole fraction and removal rate at a period of 1400 operating days for co-current and counter-current types of flow.

Fig. 7 demonstrates the partial pressure difference and hydrogen permeation rate profiles along the co-current and counter-current modes for fresh catalyst. This figure shows a higher partial pressure difference of hydrogen along the second reactor in co-current mode in comparison with counter-current mode, while an inverse behavior is observed near the reactor outlet. Also, the higher permeation rate of hydrogen is observed from 8 m to 13.2 m of the second reactor for the co-current configuration, while for lengths above 13.2 m, counter-current mode has a higher hydrogen permeation rate.

Fig. 8 shows the mole fraction and removal rates of CO over a period of 1400 operating days for both types of methanol synthesis reactor. The simulation results indicate that carbon monoxide removal is higher in the counter-current mode than in the co-current mode. Consequently, counter-current configuration is more suitable from the viewpoint of carbon monoxide removal.

6. Conclusion

Carbon monoxide is the most abundant and widely distributed air pollutant. The catalytic hydrogenation of carbon monoxide to methanol represents an effective method for preventing this side effect. In this paper, a Pd–Ag membrane was used in the second reactor of a two-stage methanol synthesis process and the effect of flow type on the performance of this system was investigated in terms of CO removal rate, catalyst activity and hydrogen permeation rate. The results show that in co-current configuration, activity of catalyst is maintained at a higher level compared with the counter-current mode because of favorable catalyst temperature profile, which results in longer catalyst life. CO removal and hydrogen permeation rate, however, are lower in this configuration due to lower heat transfer. It should be noted that hydrogen permeation has a positive effect on the rate of CO removal. Therefore, optimization of key parameters such as CO mole fraction, temperature and catalyst activity can determine which configuration of flow is more suitable for the reactor.

Appendix A. Reaction kinetics

In the methanol synthesis, three overall reactions are possible: hydrogenation of carbon monoxide, hydrogenation of carbon dioxide and reverse water–gas shift reaction, which follow as:

$$CO + 2H_2 \leftrightarrow CH_3OH \quad \Delta H_{298} = -90.55\ \text{kJ/mol} \tag{A1}$$

$$CO_2 + H_2 \leftrightarrow CO + H_2O \quad \Delta H_{298} = +41.12\ \text{kJ/mol} \tag{A2}$$

Table A.1
Reaction rate constants [33].

$K = A\exp(\frac{B}{RT})$	A	B
K_1	$(4.89 \pm 0.29) \times 10^7$	$-113{,}000 \pm 300$
K_2	$(9.64 \pm 7.30) \times 10^7$	$-152{,}900 \pm 11{,}800$
K_3	$(1.09 \pm 0.07) \times 10^7$	$-87{,}500 \pm 300$

Table A.2
Adsorption equilibrium constants [33].

$K = A\exp(\frac{B}{RT})$	A	B
K_{co}	$(2.16 \pm 0.44)\times10^{-5}$	$46{,}800 \pm 800$
K_{co2}	$(7.05 \pm 1.39)\times10^{-7}$	$61{,}700 \pm 800$
$(K_{H2O}/K_{H2}^{1/2})$	$(6.37 \pm 2.88)\times10^{-9}$	$84{,}000 \pm 1400$

Table A.3
Reaction equilibrium constants [33].

$K = \exp(\frac{B}{RT})$	A	B
K_{P1}	5139	12.621
K_{P2}	−2073	−2.029
K_{P3}	3066	10.592

$$CO_2 + 3H_2 \leftrightarrow CH_3OH + H_2O \quad \Delta H_{298} = -49.43\ \text{kJ/mol} \tag{A3}$$

Reactions (A1)–(A3) are not independent so that one is a linear combination of the other ones. In the current work, the rate expressions have been selected from Graaf et al. [33]. The rate equations combined with the equilibrium rate constants [34] provide enough information about kinetics of methanol synthesis. The correspondent rate expressions due to the hydrogenation of CO, CO_2 and the reversed water–gas shift reactions are:

$$r_1 = \frac{k_1 K_{CO}\left[f_{CO} f_{H_2}^{3/2} - f_{CH_3OH}/\left(f_{H_2}^{1/2} K_{P1}\right)\right]}{\left(1 + K_{CO} f_{CO} + K_{CO_2} f_{CO_2}\right)\left[f_{H_2}^{1/2} + (K_{H_2O}/K_{H_2}^{1/2}) f_{H_2O}\right]} \tag{A4}$$

$$r_2 = \frac{k_3 K_{CO_2}\left[f_{CO_2} f_{H_2} - f_{H_2O} f_{CO}/K_{P3}\right]}{\left(1 + K_{CO} f_{CO} + K_{CO_2} f_{CO_2}\right)\left[f_{H_2}^{1/2} + \left(K_{H_2O}/K_{H_2}^{1/2}\right) f_{H_2O}\right]} \tag{A5}$$

$$r_3 = \frac{k_2 K_{CO_2}\left[f_{CO_2} f_{H_2}^{3/2} - f_{CH_3OH} f_{H_2O}/(f_{H_2}^{3/2} K_{p2})\right]}{\left(1 + K_{CO} f_{CO} + K_{CO_2} f_{CO_2}\right)\left[f_{H_2}^{1/2} + (K_{H_2O}/K_{H_2}^{1/2}) f_{H_2O}\right]} \tag{A6}$$

The reaction rate constants, adsorption equilibrium constants and reaction equilibrium constants which occur in the formulation of kinetic expressions are tabulated in Tables A.1–A.3, respectively.

Appendix B. Auxiliary correlations

B.1. Mass transfer correlations

In the current work, mass transfer coefficients for the components have been taken from Cussler [35]. These are mass transfer coefficients between gas phase and solid phase.

$$k_{gi} = 1.17 Re^{-0.42} Sc_i^{-0.67} u_g \times 10^3 \tag{B1}$$

where the Reynolds and Schmidt numbers have been defined as:

$$Re = \frac{2R_p u_g}{\mu} \tag{B2}$$

$$Sc_i = \frac{\mu}{\rho D_m^i \times 10^{-4}} \tag{B3}$$

And the diffusivity of component i in the gas mixture is given by [36].

$$D_{im} = \frac{1 - y_i}{\sum_{i=j} \frac{y_i}{D_{ij}}} \tag{B4}$$

And also the binary diffusivities are calculated using the Fuller–Schetter–Giddins equation that is reported by Reid and his coworkers [37]. In the following Fuller–Schetter–Giddins correlation, v_{ci}, M_i are the critical volume and molecular weight of component i which are reported in Table B.1 [38].

$$D_{ij} = \frac{10^{-7} T^{3/2} \sqrt{\frac{1}{M_i} + \frac{1}{M_j}}}{P\left(v_{ci}^{3/2} + v_{cj}^{3/2}\right)^2} \tag{B5}$$

Knowing the fact that diffusion path length along the pores is greater than the measurable thickness of the pellet, for the effective diffusivity in the catalyst pore, correction should be implemented due to the structure of the catalyst. The correction factor is ratio of catalyst void fraction to the tortuosity of the catalyst (τ).

B.2. Heat transfer correlations

The overall heat transfer coefficient between circulating boiling water of the shell side and bulk of the gas phase in the tube side is given by the following correlation:

$$\frac{1}{U_{shell}} = \frac{1}{h_i} + \frac{A_i \ln\left(\frac{D_o}{D_i}\right)}{2\pi L K_w} + \frac{A_i}{A_o}\frac{1}{h_o} \tag{B6}$$

where h_i is the heat transfer coefficient between the gas phase and reactor wall and is obtained by the following correlation [39]:

$$\frac{h_i}{C_p \rho \mu}\left(\frac{C_p \mu}{K}\right)^{2/3} = \frac{0.458}{\varepsilon_B}\left(\frac{\rho u d_p}{\mu}\right)^{-0.407} \tag{B7}$$

where, in the above equation, u is superficial velocity of gas and the other parameters are those of bulk gas phase and d_p is the equivalent catalyst diameter, K is thermal conductivity of gas, ρ, μ are density and viscosity of gas, respectively and ε_B is void fraction of catalyst bed. In equation (B6), h_o is the heat transfer coefficient of boiling water in the shell side which is estimated by the following equation [40]:

$$h_o = 7.96(T - T_{sat})^3 \left(\frac{P}{P_a}\right)^{0.4} \tag{B8}$$

T and P are temperature and pressure of boiling water in the shell side, T_{sat} is the saturated temperature of boiling water at the operating pressure of shell side and P_a is the atmospheric pressure. The last term of the above equation has been considered due to effect of pressure on the boiling heat transfer coefficient. For the heat trans-

Table B.1
Molecular weight and critical volume of the components.

Component	M_i (g/mol)	v_{ci} (m^3/mol) × 10^6
CH_3OH	32.04	118.0
CO	28.01	18.0
CO_2	44.01	94.0
H_2O	18.02	56.0
H_2	2.02	6.1
CH_4	16.04	99.0
N_2	28.01	18.5

fer coefficient between bulk gas phase and solid phase (h_f), Eq. (B7) is applicable.

References

[1] Penney DG, editor. Carbon monoxide poisoning. Boca Raton (London), New York: CRC Press, Taylor & Francis Group; 2008. p. 198–9.
[2] Chung Y, Park SE, Lee K, Yanagisawa Y, Spengler JD. Determinations of personal carbon monoxide exposure and blood carboxyhemoglobin. Yonsei Med J 1994;35:420–8.
[3] Bruhl Ch, Crutzen PJ. Reductions in the anthropogenic emissions of CO and their effect on CH_4. Chemos-Global Change Sci 1999;1:249–54.
[4] Badr O, Probert SD. Carbon-monoxide concentration in the Earth's atmosphere. Appl Energy 1994;49:99–143.
[5] Badr O, Probert SD. Sinks and environmental impacts for atmospheric carbon monoxide. Appl Energy 1995;50:339–72.
[6] Chmielniak T, Sciazko M. Co-gasification of biomass and coal for methanol synthesis. Appl Energy 2003;74:393–403.
[7] Leduc S, Lundgren J, Franklin O, Dotzauer E. Location of a biomass based methanol production plant: a dynamic problem in northern Sweden. Appl Energy 2010;87:68–75.
[8] Prater DN, Rusek JJ. Energy density of a methanol/hydrogen-peroxide fuel cell. Appl Energy 2003;74:135–40.
[9] Kiso F, Arashi N. Hybrid methanol-production process. Appl Energy 1998;59:215–28.
[10] Lange JP. Methanol synthesis: a short review of technology improvements. Catal Today 2001;64:3–8.
[11] Tijm PJA, Waller FJ, Brown DM. Methanol technology developments for the new millennium. Appl Catal A: Gen 2001;221:275–82.
[12] Rahimpour MR, Ghader S. Enhancement of CO conversion in a novel Pd–Ag membrane reactor for methanol synthesis. Chem Eng Process 2004;43:1181.
[13] Rahimpour MR, Lotfinejad M. Enhancement of methanol production in a membrane two-stage reactor. Chem Eng Technol 2007;30:1062–76.
[14] Rahimpour MR, Asgari A. Modeling and simulation of ammonia removal from purge gases of ammonia plants using a Pd–Ag catalytic membrane reactor. J Hazard Mater 2008;153:557–65.
[15] Roa F, Block MJ, Way JD. The influence of alloy composition on the H_2 flux of composite Pd–Cu membranes. Desalination 2002;147:411–6.
[16] Shu J, Grandjean BPA, Neste AV, Kaliaguine S. Catalytic palladium-based membrane reactors: a review. Can J Chem Eng 1991;69:1060.
[17] Lin YM, Rei MH. Study on the hydrogen production from methanol steam reforming in supported palladium membrane reactor. Catal Today 2001;67:77–84.
[18] Rahimpour MR, Ghader S. Theoretical investigation of a Pd membrane reactor for methanol synthesis. Chem Eng Technol 2003;26:902.
[19] Chen WH, Chiu IH. Modeling of transient hydrogen permeation process across a palladium membrane. Appl Energy 2010;87:1023–32.
[20] Buxbaum RE, Kinney AB. Hydrogen transport through tubular membranes of palladium-coated tantalum and Niobium. Ind Eng Chem Res 1996;35:530.
[21] Dittmeyer R, Höllein V, Daub K. Membrane reactors for hydrogenation and dehydrogenation processes based on supported palladium. J Mol Catal A: Chem 2001;173:135–84.
[22] Gallucci F, Basilo A. Co-current and counter current modes for methanol steam reforming membrane reactor. Int J Hydrogen Energy 2006;118:237–45.
[23] Basile N, Paturzo L, Gallucci F. Co-current and counter current modes for water gas shift membrane reactor. Inst Membrane Technol 2003;82:275–81.
[24] Thunman H, Leckner B. Co-current and counter current fixed bed combustion of biofuel – a comparison. Fuel 2003;82:275–83.
[25] Rahimpour MR, Lotfinejad M. A comparison of co-current and counter-current modes of operation for an industrial dual type methanol reactor. Chem Eng Process 2007;47:1819–30.
[26] Rahimpour MR, Bayat M. Comparative study of two different hydrogen redistribution strategies along a fluidized-bed hydrogen permselective membrane reactor for methanol synthesis. Ind Eng Chem Res 2010;49:472–80.
[27] Chang T, Rousseau RW, Kilpatrick PK. Methanol synthesis reactions: calculations of equilibrium conversions using equations of state. Ind Eng Chem Process Des Dev 1986;25:477–81.
[28] Klier K, Chatikavanij V, Herman RG, Simmons GW. Catalytic synthesis of methanol from CO/H_2. IV. Effects of carbon dioxide. J Catal 1982;74:343.
[29] Hanken L. The Norwegian University of Science and Technology. Master's thesis. 1995.
[30] Hara S, Xu WC, Sakaki K, Itoh N. Kinetics and hydrogen removal effect for methanol decomposition. Ind Eng Chem Res 1999;38:488–92.
[31] Barbieiri G, Maio FDi. Simulation of the methane steam reforming process in a catalytic Pd membrane reactor. Ind Eng Chem Res 1997;36:2121–7.
[32] Shu J, Grandjean BPI, Kaliaguine S. Methane steam reforming in asymmetric Pd–Ag and Pd–Ag/porous SS membrane reactors. Appl Catal A: Gen 1994;119:305–25.
[33] Graaf GH, Scholtens H, Stamhuis EJ, Beenackers AACM. Intra-particle diffusion limitations in low-pressure methanol synthesis. Chem Eng Sci 1990;45:773.
[34] Graaf GH, Sijtsema PJJM, Stamhuis EJ, Joosten GEH. Chemical equilibria in methanol synthesis. Chem Eng Sci 1986;41:2883.
[35] Cussler EL. Diffusion-mass transfer in fluid systems. Cambridge: Cambridge University Press; 1984.
[36] Wilke CR. Estimation of liquid diffusion coefficients. Chem Eng Prog 1949;45:218.
[37] Reid RC, Sherwood TK, Prausnitz J. The properties of gases and liquids. 3rd ed. New York: McGraw-Hill; 1977.
[38] Hartig F, Keil FJ. Large-scale spherical fixed bed reactors, model. Optim Ind Eng Chem Res 1993;32:424.
[39] Smith JM. Chemical engineering kinetics. New York: McGraw-Hill; 1980.
[40] Holman JP. Heat transfer. New York: McGraw-Hill; 1989.